IOP Publishing Journal of Micromechanics and Microengineering

J. Micromech. Microeng. **17** (2007) 1583–1592 doi:10.1088/0960-1317/17/8/022

Capacitive detection in resonant MEMS with arbitrary amplitude of motion

Alexander A Trusov and Andrei M Shkel

Mechanical and Aerospace Engineering Department, MicroSystems Laboratory EG2110, University of California, Irvine, CA 92697, USA

E-mail: atrusov@uci.edu and ashkel@uci.edu

Received 7 May 2007, in final form 8 June 2007
Published 13 July 2007
Online at stacks.iop.org/JMM/17/1583

Abstract

Detection of motion with parallel plate capacitors is commonly used in MEMS; small amplitude of motion is typically assumed. In this paper, we derive precise and constructive equations for the case of parallel plate capacitive detection of arbitrary amplitude of motion. These equations are solved in closed form without using a small displacement assumption. A precise relation between the amplitude of the mechanical motion and the amplitude of the electrical sensing signals is obtained, which allows us to eliminate the nonlinearity error of parallel plates. To illustrate the theoretical findings, MEMS test structures were designed and fabricated. Experiments confirm the developed theory. The formulated algorithms of detection are especially valuable for capacitive detection of large amplitudes of periodic motion in dynamic MEMS sensors and actuators.

1. Introduction

Nonlinearity of parallel plates capacitance as a function of displacement presents a challenge in both electrostatic actuation and capacitive detection. Issues of large amplitude parallel plate actuation were extensively studied previously, for example in [1–3]. The challenges of large amplitude detection using parallel plates were not sufficiently studied in the literature. The problem was introduced in [4], and this paper presents a detailed analytical and experimental analysis of the problem.

Resonators [5], gyroscopes [6] and chemical sensors [7] utilize resonant phenomena in their operation. In these devices, the vibratory motion needs to be initiated, detected and controlled. Capacitive phenomena are commonly used for transduction in vibratory MEMS devices due to the ease of fabrication, low sensitivity to temperature changes and other practical advantages [8, 9].

Capacitive sensing of vibratory motion is often based on measuring the current induced by the relative motion of capacitive electrodes, where a variable sense capacitor is formed between a movable mass and anchored electrodes. A predefined dc or ac potential difference is maintained across the sense capacitor [10–12]; the motion induces change of the capacitance, which results in a flow of current. Signal processing, such as amplitude demodulation [13], is used to extract the motional amplitude from the pick-up signal. Parallel plates and lateral combs are the two most common configurations of capacitive structures used to actuate and detect motion in resonant MEMS devices. Typically, for the same real estate, parallel plate sense capacitors provide much higher capacitive gradient and thus sensitivity [14]. However, unlike lateral combs, parallel plates generate sense signal that is nonlinear with motional amplitude [13]. Historically, this limited the use of parallel plate capacitive detection to small amplitudes of motion, e.g., in sense modes of vibratory gyroscopes [15].

Electromechanical amplitude modulation (EAM) is an often used capacitive detection technique. It is based on amplitude modulation of the motional signal by an ac probing voltage (carrier) and allows for frequency domain separation between the useful informational signals and feed-through of the driving voltages [16, 17]. The conventional linear EAM can be used for either lateral comb sense capacitors or for small displacement parallel plate capacitors.

This work is concerned with the application of an EAM technique to the parallel plate detection of motion in vibratory devices with arbitrary motional amplitudes. In section 2, we analytically derive Fourier series for the parallel plate detection current. Section 3 focuses on the main pair of

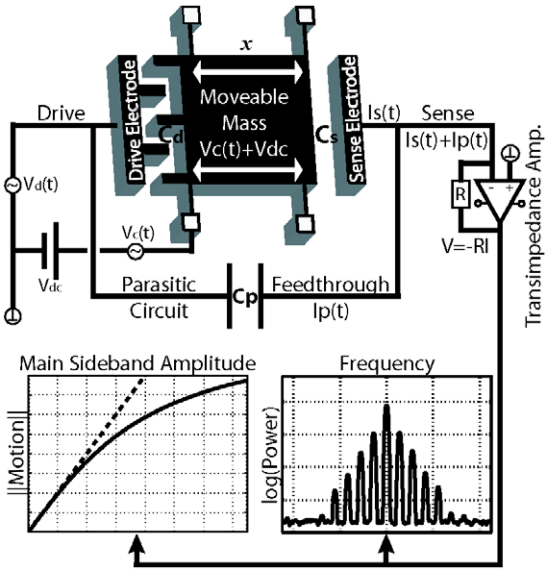

Figure 1. Schematic of a capacitive MEMS resonator.

the informational sidebands. In this section, a relationship between the amplitudes of the sidebands and the amplitude of motion is obtained and solved in the closed form. The theoretical results are experimentally confirmed in section 4. In section 5, we discuss the application of the obtained results to the cases of differential EAM and detection with a pure dc probing voltage. Section 6 concludes the paper.

2. Capacitive detection of periodic motion

2.1. Electromechanical model

Figure 1 shows a general schematic of a capacitive micro-resonator, a basic element of various micro-devices. The electro-mechanical diagram includes the mechanical resonator, the electrostatic drive and capacitive sense electrodes. The movable mass m of the resonator is suspended with a spring k and is constrained to move only along the horizontal x-axis. The variable sense capacitance is defined as $C_s(x)$, and the drive capacitance as $C_d(x)$, where x is the displacement. Typically in MEMS devices, drive and sense terminals are not completely isolated, but are electrically coupled by stray parasitic capacitors and resistors [10, 12, 17]. In this paper, we assume without loss of generality that the parasitic circuit consists of a single lumped capacitor C_p, which couples the drive and sense electrodes.

The ac driving voltage $V_d(t) = v_d \cos(\omega_d t)$ is applied to the drive electrode and a dc bias V_{dc} is applied to the moveable mass (all voltage values are referenced with respect to a common ground). The motion of the resonator is governed by

$$\ddot{x} + \frac{\omega_n}{Q}\dot{x} + \omega_n^2 x = \frac{1}{2m}\frac{\partial C_d(x)}{\partial x}(V_{\text{dc}} - V_d(t))^2, \tag{1}$$

where $\omega_n = \sqrt{\frac{k}{m}}$ is the undamped natural frequency and Q is the quality factor. Using trigonometric identities, the equation of motion can be written in the form

$$\ddot{x}(t) + \frac{\omega_n}{Q}\dot{x}(t) + \omega_n^2 x = \frac{\partial C_d(x)}{2m\partial x} \times \left\{\left(V_{\text{dc}}^2 + \frac{1}{2}v_d^2\right) - 2V_{\text{dc}}v_d\cos(\omega_d t) - \frac{1}{2}v_d^2\sin(2\omega_d t)\right\}. \tag{2}$$

If we assume a linear drive capacitor, such as a lateral comb structure, with a constant capacitive gradient, $\partial C/\partial x = \text{const}$, then the motion of the resonator is governed by a linear time-invariant (LTI) system with three simultaneous inputs: a static force and two sinusoidal forces at ω_d and $2\omega_d$ frequencies, respectively. If we further assume that $v_d \ll V_{\text{dc}}$, and ω_d is close to the resonant frequency of the device, then the effect of the $\frac{1}{2}v_d^2\sin(2\omega_d t)$ forcing term is negligible and the resonator's displacement $x(t)$ relative to the steady-state static displacement can be expressed as

$$x(t) = \|x\|\sin(\omega_d t + \phi), \tag{3}$$

where $\phi = \phi(\omega_d)$ represents a phase lag in the transfer function of the resonator. The results developed in this paper are valid for all vibratory structures with quasi-sinusoidal motion, independent of type of forcing, such as electrostatic in the case of gyroscope drive mode or inertial in the case of gyroscope sense mode.

The sense capacitor C_s is formed between the movable mass and the fixed sense electrode. The sense electrode is connected to the inverting input of an operational amplifier, which is configured as a trans-impedance amplifier [18]. During the motion, the sense capacitance $C_s(x)$ changes, causing a flow of motional current $I_s = \mathrm{d}(C_s V_s)/\mathrm{d}t$, where V_s is the sensing voltage across the sense capacitor. The total pick-up current $I(t) = I_s(t) + I_p(t)$ consists of both the motional and the parasitic currents and is converted to the final output voltage $V(t)$ with trans-impedance gain $-R$. The parasitic current is induced by the drive voltage V_d and therefore has the same frequency ω_d. In this work, we assume that the total sensing voltage $V_s(t) = V_{\text{dc}} + V_c(t)$ is composed of a dc component V_{dc} and an ac component $V_c = v_c\sin(\omega_c t)$, called carrier. Particular cases when either dc or ac component of the sense voltage is zero are discussed in section 5. Utilization of an ac carrier voltage results in an amplitude modulation of the motional signal, known as electromechanical amplitude modulation (EAM).

According to the laws of electrostatics, the total pick-up current that flows through the feed-back resistor of the trans-impedance amplifier is

$$I(t) = \frac{\mathrm{d}}{\mathrm{d}t}[V_d(t)C_p + (V_c(t) + V_{\text{dc}})C_s(t)]. \tag{4}$$

The sense capacitance $C_s(x(t)) = C_s(t)$ is a function of time when the resonator is vibrating according to equation (3). Depending on the particular form of the sense capacitance $C_s(x)$, equation (4) can be expanded to describe specific properties of the pick-up signal. Analysis of the pick-up signal and its spectral properties is the focus of our discussion. First, we carry out the derivations for a classical linear case of lateral combs. We then derive the properties of the output current for the case of parallel plates and analyze the nonlinear effects.

2.2. Motion detection with lateral combs

In this section, we review widely known properties of linear EAM [10, 17]. The results will be used later in the paper for comparative study of the nonlinear case. In the conventional linear case, the sense capacitor $C_s(t)$ is formed by a pair of lateral fingers [19]. We denote media permittivity by ε, the initial comb fingers penetration at rest by d, comb height (i.e., thickness of device layer) by y, gap between inter-digited fingers by g and the total number of finger overlap pairs by N. For this type of electrodes, the sense capacitance is linear with respect to displacement x:

$$C_s(t) = \frac{\varepsilon(d + x(t))yN}{g} = \frac{\varepsilon dyN}{g}\left(1 + \frac{x(t)}{d}\right). \tag{5}$$

We introduce the dimensionless amplitude of oscillation $x_0 = \|x\|/d$ and the nominal sense capacitance $C_{\text{sn}} = \varepsilon dyN/g$. The time-varying sense capacitance can be now expressed as

$$C_s(t) = C_{\text{sn}}(1 + x_0 \sin(\omega_d t + \phi)). \tag{6}$$

The sense capacitance varies sinusoidally; the amplitude of its variation, $\|C_s\| = C_{\text{sn}}x_0$, is proportional to the amplitude of motion, $\|x\|$. The total EAM-modulated pick-up current is calculated by substituting equation (6) into equation (4):

$$\begin{aligned} I(t) = {} & -C_p v_d \omega_d \sin(\omega_d t) \\ & + C_{\text{sn}} V_{\text{dc}} x_0 \omega_d \cos(\omega_d t + \phi(\omega_d)) + C_{\text{sn}} v_c \omega_c \cos(\omega_c t) \\ & + \tfrac{1}{2}\|C_s\| v_c(\omega_c + \omega_d) \sin((\omega_c + \omega_d)t + \phi) \\ & - \tfrac{1}{2}\|C_s\| v_c(\omega_c - \omega_d) \sin((\omega_c - \omega_d)t - \phi). \end{aligned} \tag{7}$$

Figure 2(*a*) shows a simulated power spectral density (PSD) plot of a typical linear EAM pick-up signal and illustrates its important features. In this particular example, the device was driven into resonance at $f_d = \omega_d/(2\pi) = 550$ Hz frequency, and the carrier frequency was $f_c = \omega_c/(2\pi) = 20$ kHz. The pick-up current has four discrete frequency components. Amplitudes of the EAM sidebands at frequencies $\omega_c \pm \omega_d$ are proportional to the sense capacitance amplitude and thus to the motional amplitude. The two signals at ω_d and ω_c frequencies are parasitic feed-through of the drive voltage, $V_d(t)$, and the carrier signal, $V_c(t)$. By demodulating the EAM signal, the amplitudes and phases of the sidebands are extracted. Amplitudes of the sidebands are proportional to the amplitude of motion.

2.3. Motion detection with parallel plates

This section studies application of an EAM detection scheme to the case of parallel plate sense capacitors with arbitrary amplitude of motion. Let us consider a variable sense capacitor, $C_s(t)$, formed by a pair of movable and anchored parallel plate electrodes. Let us denote the initial gap between plates at rest by g, overlap length of individual parallel plate pairs by L and plate height (i.e., structural layer thickness) by y. The total overlap area in the sense capacitor is given by $A = NLy$, where N is the number of parallel plate pairs in the capacitor. The total variable sense capacitance for the sinusoidal mode of motion equation (3) is

$$C_s(t) = \frac{\varepsilon A}{g - x(t)} = \frac{\varepsilon A}{g}\frac{1}{1 - \frac{\|x\|}{g}\sin(\omega_d t)}, \tag{8}$$

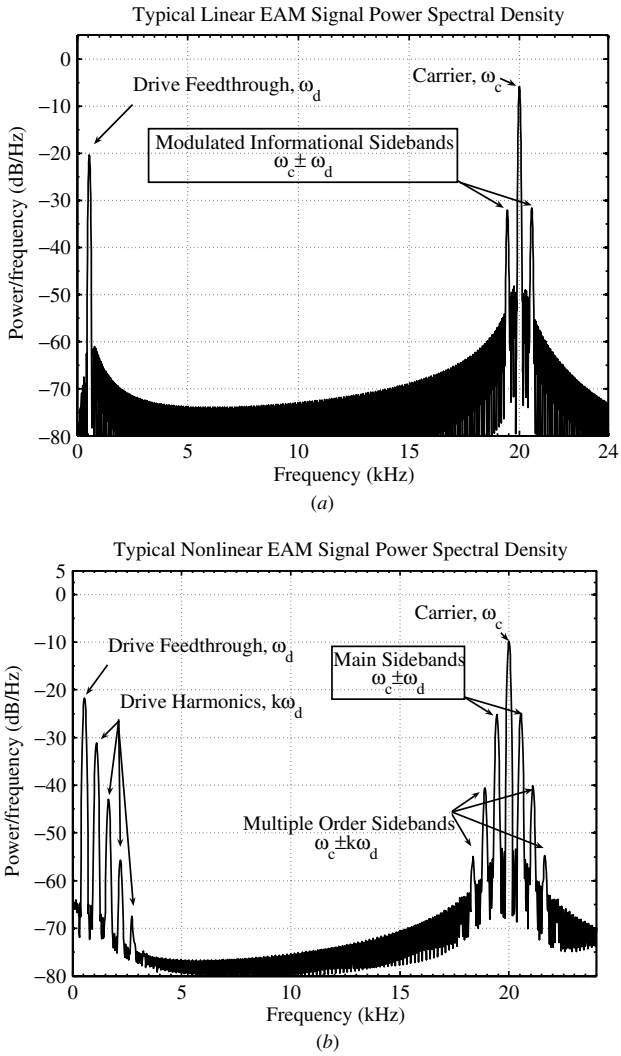

Figure 2. Typical spectra of EAM pick-up signals: (*a*) using lateral comb capacitors (linear case) and (*b*) using parallel plate capacitors (nonlinear case).

where the phase of motion, ϕ, is omitted without any loss of generality.

We introduce the nominal sense capacitance $C_{\text{sn}} = \varepsilon A/g$ and the dimensionless amplitude of motion $x_0 = \|x\|/g < 1$ (normalized with respect to the initial gap between parallel plates). From equation (8), the sense capacitance is

$$C_s(t) = C_{\text{sn}}\frac{1}{1 - x_0 \sin(\omega_d t)}. \tag{9}$$

Since physically $x_0 < 1$, we use Taylor series expansion method to obtain a precise infinite series expansion for the nonlinear parallel plate capacitance:

$$C_s(t) = C_{\text{sn}} \sum_{n=0}^{\infty} (x_0 \sin(\omega_d t))^n. \tag{10}$$

Next, in order to obtain Fourier series of $C_s(t)$ we use Euler's formula to convert from powers of harmonics to harmonics of multiple frequencies:

$$\sin(\omega_d t) = \frac{e^{i\omega_d t} - e^{-i\omega_d t}}{2i}, \tag{11}$$

and Newton's binomial theorem to expand these terms:

$$(a+b)^n = \sum_{k=0}^{n} C_{(n,k)} a^{n-k} b^n, \tag{12}$$

where Newton's binomial coefficients are defined as $C_{(n,k)} = \frac{n!}{k!(n-k)!}$. We substitute harmonic terms into equation (10) with complex exponents using equation (11). Then, each term in the sum can be expanded according to equation (12). Terms of odd and even orders are arranged in two distinct groups. Finally, the inverse equation (11) is used to convert terms back from complex exponents to the regular sine and cosine functions. The normalized sense capacitance can be derived as

$$\begin{aligned}\frac{C_s(t)}{C_{\text{sn}}} &= \sum_{n=0}^{\infty} {x_0}^{2n} \frac{(-1)^n}{2^{2n-1}} \sum_{k=0}^{n} (-1)^{n-k} C_{(2n,n-k)} \cos(2k\omega_d t) \\ &+ \sum_{n=0}^{\infty} {x_0}^{2n+1} \frac{(-1)^n}{2^{2n}} \sum_{k=0}^{n} (-1)^{n-k} \\ &\times C_{(2n+1,n-k)} \sin((2k+1)\omega_d t).\end{aligned} \tag{13}$$

Equation (13) gives a power series expansion of the sense capacitance $C_s(t)$ with respect to the normalized motional amplitude x_0. The coefficients of each x_0 power term are formed by the finite sums of drive frequency harmonics, $(n\omega_d)$, with binomial coefficient weights. We then swap the order of the summations by algebraically regrouping terms in equation (13) to obtain the Fourier series of the variable sense capacitance:

$$\begin{aligned}\frac{C_s(t)}{C_{\text{sn}}} &= \sum_{k=0}^{\infty} \cos(2k\omega_d t) \sum_{n=k}^{\infty} \left\{ \frac{(-1)^{2n-k}}{2^{2n-1}} C_{(2n,n-k)} x_0^{2n} \right\} \\ &+ \sum_{k=0}^{\infty} \sin((2k+1)\omega_d t) \sum_{n=k}^{\infty} \left\{ \frac{(-1)^{2n-k}}{2^{2n}} C_{(2n+1,n-k)} x_0^{2n+1} \right\}.\end{aligned} \tag{14}$$

The Fourier coefficients, functions $p_k(x_0)$, are given by the following infinite Taylor series:

$$\begin{aligned} p_0(x_0) &= \sum_{n=0}^{\infty} \frac{C(2n,n)}{2^{2n}} x_0^{2n} = \frac{1}{\sqrt{1-x_0^2}}, \\ &\text{and for } k = 0, 1, 2, \ldots \infty \\ p_{2k+1}(x_0) &= (-1)^k \sum_{n=k}^{\infty} \left\{ \frac{C(2n+1, n-k) x_0^{2n+1}}{2^{2n}} \right\}, \\ p_{2k}(x_0) &= (-1)^k \sum_{n=k}^{\infty} \left\{ \frac{C(2n, n-k) x_0^{2n}}{2^{2n-1}} \right\}. \end{aligned} \tag{15}$$

Then, the Fourier series expansion of the sense capacitance is obtained from equations (14) and (15) as

$$\begin{aligned} C_s(t) &= C_{\text{sn}} \sum_{k=0}^{\infty} p_{2k}(x_0) \cos(2k\omega_d t) \\ &+ C_{\text{sn}} \sum_{k=0}^{\infty} p_{2k+1}(x_0) \sin((2k+1)\omega_d t). \end{aligned} \tag{16}$$

Finite-order Taylor polynomial approximations for the Fourier coefficients, $p_k(x_0)$, can be obtained from equation (15) as

$$\begin{aligned} p_0(x_0) &= 1 + \tfrac{1}{2}x_0^2 + \tfrac{3}{8}x_0^4 + \tfrac{5}{16}x_0^6 + \underline{O}\left(x_0^8\right) \\ p_1(x_0) &= x_0 + \tfrac{3}{4}x_0^3 + \tfrac{10}{16}x_0^5 + \tfrac{35}{64}x_0^7 + \underline{O}\left(x_0^9\right) \\ p_2(x_0) &= -\tfrac{1}{2}x_0^2 - \tfrac{1}{2}x_0^4 - \tfrac{15}{35}x_0^6 - \underline{O}\left(x_0^8\right) \\ p_3(x_0) &= -\tfrac{1}{4}x_0^3 - \tfrac{5}{16}x_0^5 - \tfrac{1}{4}x_0^7 - \underline{O}\left(x_0^9\right) \\ p_4(x_0) &= \tfrac{1}{8}x_0^4 + \tfrac{3}{16}x_0^6 + \underline{O}\left(x_0^8\right). \end{aligned} \tag{17}$$

Equation (16) shows that when parallel plates are used to sense sinusoidal motion, the time-varying sense capacitance contains an infinite number of drive frequency harmonics; functions $p_k(x_0)$ define the amplitudes of these harmonics. Specifically, $p_1(x_0)$ defines the amplitude of the main, first-order, harmonic $C_{\text{sn}} \sin(\omega_d t)$. Analysis of $p_1(x_0)$ is essential for the study of the parallel plate sensing nonlinearities and is presented in section 3.

In order to calculate the total output signal, we consider modulation of each harmonic individually. The total EAM-modulated pick-up current is calculated by substituting equation (16) into equation (4):

$$\begin{aligned} I(t) &= -C_p v_d \omega_d \sin(\omega_d t) + C_{\text{sn}} v_c \omega_c p_0(x_0) \cos(\omega_c t) \\ &+ C_{\text{sn}} V_{\text{dc}} \omega_d \begin{Bmatrix} \sum_{k=0}^{\infty} (2k+1) p_{2k+1}(x_0) \cos((2k+1)\omega_d t) \\ -\sum_{k=1}^{\infty} 2k p_{2k}(x_0) \cos(2k\omega_d t) \end{Bmatrix} \\ &+ \frac{1}{2} C_{\text{sn}} v_c \sum_{k=0}^{\infty} p_{2k+1}(x_0) \begin{bmatrix} \omega_{(2k+1)} \sin(\omega_{(2k+1)} t) \\ -\omega_{-(2k+1)} \sin(\omega_{-(2k+1)} t) \end{bmatrix} \\ &+ \frac{1}{2} C_{\text{sn}} v_c \sum_{k=1}^{\infty} p_{2k}(x_0) \begin{bmatrix} \omega_{(2k)} \cos(\omega_{(2k)} t) \\ +\omega_{(-2k)} \cos(\omega_{(-2k)} t) \end{bmatrix}, \end{aligned} \tag{18}$$

where $\omega_k = \omega_c + k\omega_d$ is the frequency of a sideband of order k. The equation gives the Fourier series for the total pick-up signal for the case of parallel plate capacitive detection of sinusoidal motion. The result completes the analytical derivations. In order to verify correctness of the derived Fourier series for the parallel plate capacitance, $C_s(t)$, and sense current, $I(t)$, detailed computer simulations were performed. Equations (8) and (4) were used to directly compute $C(t)$ and $I(t)$, respectively; the finite-order Fourier approximations were computed according to (16) and (18). Figures 3(*a*) and (*b*) show typical results of such numerical experiments confirming correctness of the derived mathematical model of parallel plate detection.

Figure 2(*b*) shows the frequency domain representation of the parallel plate EAM pick-up signal and illustrates its important features. There exists an infinite number of informational sidebands. The frequencies of these sidebands are given by $\omega_k = \omega_c \pm k\omega_d$, where $k = 1, 2, 3, \ldots \infty$ is the sideband order. The amplitudes of the sidebands are given by the nonlinear functions of the motional amplitude, $p_k(x_0)$, equation (15). The parallel plate EAM signal also contains power at multiples of the drive frequency $k\omega_d$ if there is a dc voltage component across the sensing capacitor. The spectral content of the parallel-plate-modulated signal is important for correct implementation of the EAM scheme; it affects the choice of the carrier frequency, design of demodulators and specifications of pass-band filters.

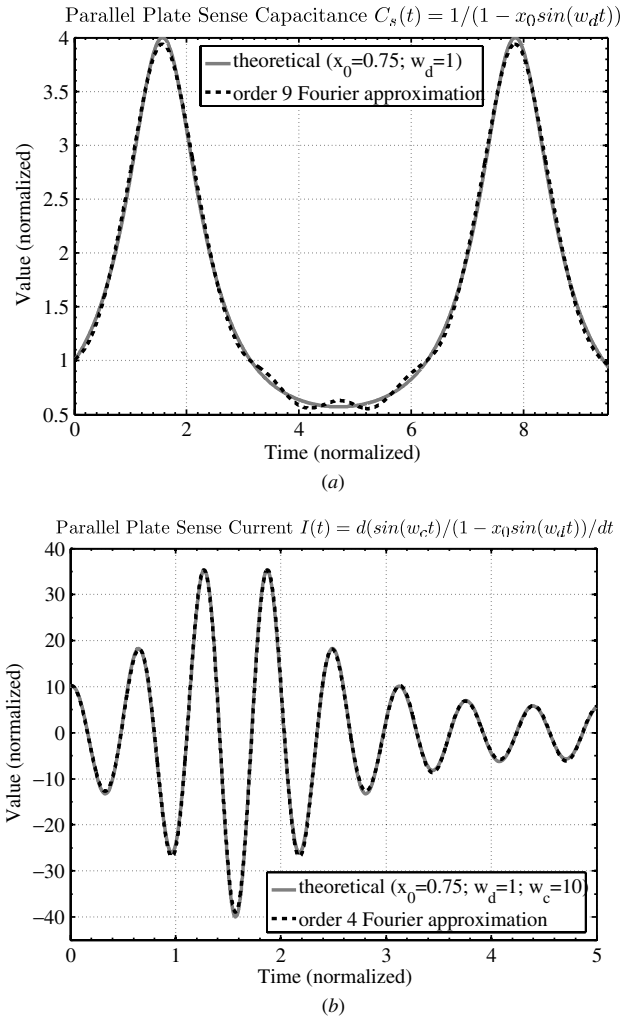

Figure 3. Numerical verification of the derived Fourier series: (*a*) parallel plate capacitance and (*b*) parallel plate current.

3. Nonlinearity of main sidebands

3.1. Demodulation

The final step of the EAM detection scheme is demodulation [10, 17]. Demodulation consists of mixing and pass-band filtering of the signals in order to generate a dc signal proportional to the amplitude of one or both main (first-order) sidebands. In the linear case, the sidebands are proportional to the amplitude of motion, and the demodulated dc signal provides a linear measurement of this motional amplitude. In the case of parallel plate sense capacitors, however, the relationship between the motional amplitude and the amplitude of the sidebands is not linear. According to equation (18), the amplitudes of the left and right main EAM sidebands are given by $\frac{1}{2}C_{sn}v_c(\omega_c \mp \omega_d)p_1(x_0)$. The amplitude-dependent nonlinearity of the sidebands is given by $p_1(x_0)$, while the term $\frac{1}{2}C_{sn}v_c(\omega_c \mp \omega_d)$ defines the proportionality coefficient. Therefore, we call $p_1(x_0)$ the normalized amplitude of the sideband.

Depending on the amplitude of motion, there are two considerations when parallel plates are used for capacitive detection. First, when the amplitude of motion is small, linear approximation can be assumed by neglecting all nonlinearities of the pick-up signal. It is important to estimate the systematic error of the linearization approach. Second, when the amplitude of motion is large, the complete nonlinear model should be used to correctly extract value of the motional amplitude from the nonlinear pick-up signal. Both the linearization error and complete nonlinear model are studied in the following subsections.

3.2. Closed-form solution

It is possible to derive a closed-form solution for the main sideband normalized amplitude, $p_1(x_0)$. From equation (15), $p_1(x_0)$ was found to satisfy the following differential equation:

$$[x_0 p_1(x_0)]'_{x_0} = 2x_0 + x_0\big[x_0^2 p_1(x_0)\big]'_{x_0} \quad \Leftrightarrow$$
$$\big(x_0^3 - x_0\big)p_1'(x_0) + \big(2x_0^2 - 1\big)p_1(x_0) + 2x_0 = 0. \tag{19}$$

The solution of this equation can be found as

$$p_1(x_0) = 2\frac{1 - \sqrt{1 - x_0^2}}{x_0\sqrt{1 - x_0^2}}. \tag{20}$$

The obtained closed-form solution provides a convenient way to analyze $p_1(x_0)$ numerically and analytically. Solving equation (20) for $x_0(p_1)$ yields three solutions. Since $p_1(x_0)$ is a monotonically increasing function on [0,1), only one of the solutions is real, while the other two are complex. The unique real solutions is

$$x_0(p_1) = \frac{\big(w^2 - 12 + p_1^2 - p_1 w\big)\big(w^2 - 12 + p_1^2 + 2pw\big)}{18 p_1 w^2},$$
$$\text{where} \quad w = \Big(72p_1 - p_1^3 + 6\big(48 + 132p_1^2 - 3p_1^4\big)\Big)^{\frac{1}{6}}. \tag{21}$$

This closed-form solution can be used to compensate for the nonlinearity of the main, first-order, informational sidebands of the parallel plate EAM signal. It was found that a very precise and relatively simple approximation of $x_0(p_1)$ is given by

$$x_0(p_1) \approx \frac{kp_1(p_1 - a)}{p_1^2 + bp_1 + c}, \qquad \text{where} \quad a = -1.222,$$
$$b = 0.7812, \qquad c = 1.007, \qquad k = 0.822. \tag{22}$$

The relative error between the true $x_0(p_1)$ and the rational approximation equation (22) is smaller than 1% in a wide range ($p_1 \in [0, 4.5] \Longleftrightarrow x_0 \in [0, 0.95]$).

3.3. Linearization error

Figure 4(*a*) shows the normalized amplitude $p_1(x_0)$ of the main (first-order) sidebands as a function of the gap-normalized amplitude of motion x_0; the linearization of $p_1(x_0)$ is also shown in the plot. The nonlinearity of the parallel plate sense capacitor causes the actual sidebands to be larger than predicted by linear theory of operation. The discrepancy increases for larger amplitudes of motion. The relative error between the nonlinear amplitude of the main sidebands $p_1(x_0)$

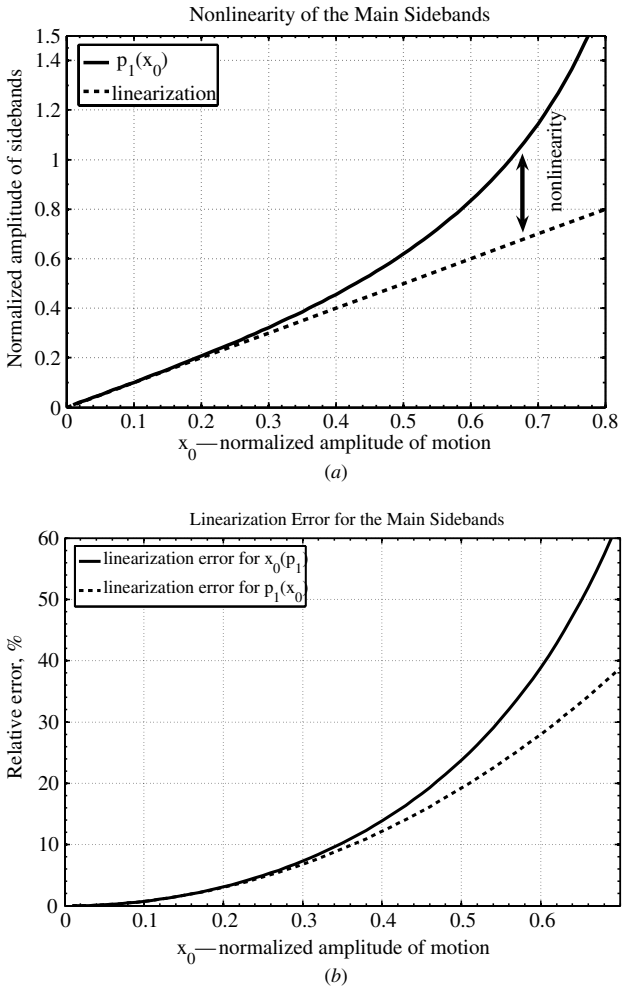

Figure 4. Nonlinearity of the main (first-order) sidebands in parallel plate EAM: (*a*) $p_1(x_0)$ and its linearization and (*b*) linearization errors.

and its linearization are shown in figure 4(*b*). According to equation (20), this linearization error is computed as

$$e_{p_1(x_0)} = \frac{|p_1(x_0) - x_0|}{p_1(x_0)} = 1 - \frac{{x_0}^2\sqrt{1-{x_0}^2}}{2-2\sqrt{1-{x_0}^2}}. \quad (23)$$

The linear approximation shows a 3% error for normalized amplitude of motion $x_0 = 0.2$; the error is 7% for $x_0 = 0.3$, more than 12% for $x_0 = 0.4$ and the error is almost 20% for $x_0 = 0.5$.

Let us consider a resonating MEMS device with parallel plate EAM sensing of the motion. The amplitudes of the main informational sidebands are used to measure the motional amplitudes. Assuming this to be a linear measurement, which is a good approximation for the lateral comb case but not for the parallel plate case, leads to a significant overestimation of the actual motional amplitude value. The error of this overestimation is caused by the nonlinearity of the inverse function $x_0(p_1)$ and is shown in figure 4(*b*). Using Taylor series expansion it can be shown that $x_0 \approx p_1(x_0)$ is the linear approximation for any given x_0. Accordingly, the error of the linearization is given by

$$e_{x_0(p_1)} = \frac{|x_0 - p_1(x_0)|}{x_0} = \frac{2}{{x_0}^2\sqrt{1-{x_0}^2}} - 2{x_0}^{-2} - 1, \quad (24)$$

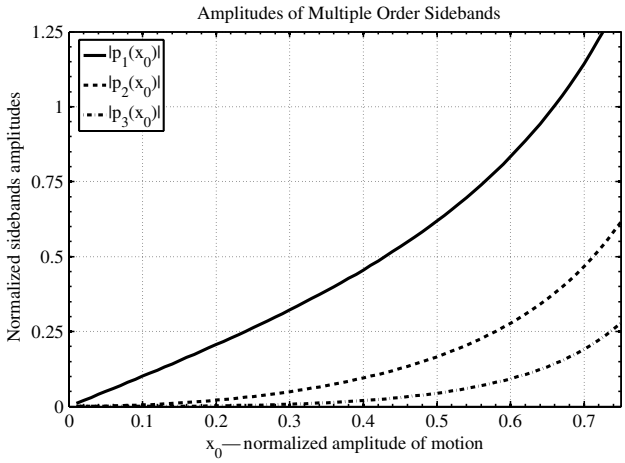

Figure 5. Normalized amplitudes of the first three sidebands.

and is even more drastic than $e_{p_1(x_0)}$. For instance, the linear measurement error is approximately 24% for $x_0 = 0.5$.

3.4. Nonlinear measurement

The linearization error, $e_{x_0(p_1)}$, is always present in the estimation of motional amplitude if the linearization is used. Compensation for this nonlinearity error is essential for accurate operation of the parallel plate detection schemes. A nonlinear calculation for the motional amplitude should be used to compensate for the overestimations and provide an accurate measurement of the actual amplitude of motion. There are several approaches to accurate calculation of motional amplitude $x_0(p_1)$ based on measured sideband amplitude p_1. First, equation (20) can be used to pre-compute a look-up table of x_0 and p_1 pairs. Alternatively, a closed form equation (21) can be used to perform direct calculation of $x_0(p_1)$. Additionally, a simple rational approximation equation (22) can be used to estimate $x_0(p_1)$ with less than 1% error.

3.5. Sinusoidal and periodic motion

The presented results on parallel plate nonlinear detection were derived using the assumption of sinusoidal motion. However, the main results on compensation of the first-order sidebands nonlinearity are more general. Let us consider an arbitrary periodic motion of the structure. Depending on a particular waveform, the motion can be decomposed into a sum of harmonics using Fourier series. However, the amplitudes of the main EAM sidebands depend only on the first harmonic component of the motion. Thus, equation (21) and its variations can be directly applied to measure amplitude of main motional harmonic in devices with arbitrary periodic motion.

Higher order sidebands ($k = 2, 3, \ldots$), see figure 2(*b*), also carry useful information and can be potentially utilized in parallel plate detection schemes. However, this approach will be limited to the case of quasi-sinusoidal motion. Amplitudes of the first three order sidebands as functions of the motional amplitude are shown in figure 5 and are later compared to the experimentally measured values.

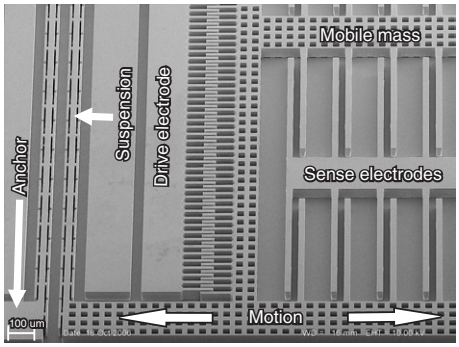

(*a*)

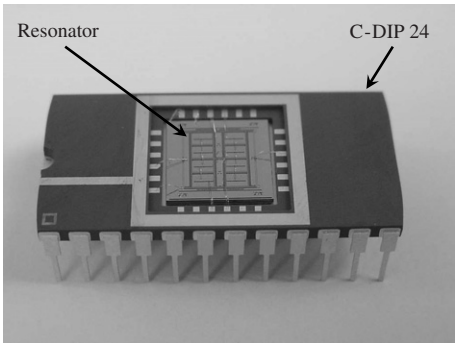

(*b*)

Figure 6. Fabricated and packaged test resonator: (*a*) SEM micrograph of a quarter of the fabricated device and (*b*) photograph of the packaged and wirebonded device.

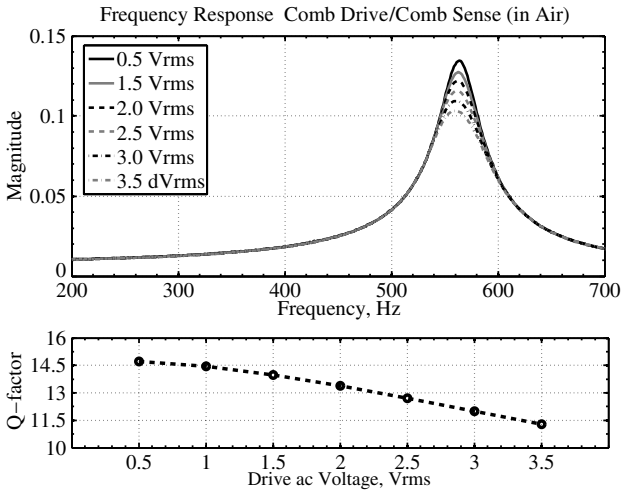

Figure 7. Characterization of the test structure in air.

Table 1. Parameters of the test device.

Parameter (units)	Value
Device thickness (μm)	50
Device resistivity (Ω cm)	0.01–0.03
Device layer type	P/B, (1-0-0)
Resonant frequency (Hz)	555
Mass (kg)	9.664×10^{-7}
Stiffness (N m^{-1})	11.75
Total plate capacitance (pF)	2×0.7
Parallel plate gap (μm)	25
Lateral comb capacitance (pF)	4×0.7
Lateral comb gap (μm)	5

4. Experimental demonstration

4.1. Fabrication of test structures

In order to verify the theoretical findings of this paper several test structures were designed, fabricated and characterized. The devices were capacitive MEMS resonators with lateral comb drive capacitors, and lateral comb and parallel plate sense capacitors. The fabrication was done using an in-house wafer-level SOI process. SOI wafers with a highly conductive 50 μm thick device layer were used. AZ-4620 photoresist was spin-coated onto the wafers and patterned using a chrome-on-glass mask and a Karl Suss MA-6 exposure system. The exposed wafers were developed using water-diluted AZ-400K developer. Then, the wafers with the photoresist mask were subjected to a deep reactive ion etching (DRIE) using a Surface Technology Systems (STS) tool. The minimum gap feature of the process was 5 μm and minimum structural feature was 8 μm. The nominal capacitive gap in the parallel plate sense structure was 25 μm; the relatively large gaps were chosen purely for easier optical tracking of motion during the experiments. An SEM image of a fabricated test resonator is shown in figure 6(*a*). After the fabrication, the individual devices were packaged in C-DIP24 packages and wirebonded (figure 6(*b*)). Table 1 summarizes the main properties of the fabricated test structures.

4.2. Structural characterization

Device characterization was performed in air using lateral comb capacitors for drive and sense. The biasing scheme similar to that shown in figure 1 was used. A sum of the driving 60 V dc and 0.5–3.5 $V_{\rm rms}$ ac voltages was applied to the fixed comb electrode. The ac component was generated by an HP 35 665A dynamic signal analyzer, which was running in a swept-sine mode. The carrier voltage of 5 $V_{\rm rms}$ ac at 20 kHz was applied to the moving mass. The carrier ac voltage was generated by a digital lock-in amplifier, AMETEK Advanced Measurement Technology Signal Recovery Model 7265. The pick-up current from the sensing capacitor was pre-amplified by a trans-impedance amplifier with a 0.5 MΩ gain. The demodulation at the carrier frequency was performed by the lock-in amplifier. Then, the signal was fed back into the signal analyzer to acquire frequency response data. This characterization method was described in detail, for example, in [10].

Figure 7 (top) shows frequency responses (defined as a ratio of the output signal to the driving voltage) obtained at different levels of the driving ac voltage and thus motional amplitudes. The resonant frequency was approximately 555 Hz. The effective quality factor Q in air was observed to depend on the amplitude of motion and ranged from 15 to 12.5 (figure 7 (bottom)). This amplitude-dependent change of the frequency response is attributed to amplitude-dependent damping; however, the discussion about the exact physical mechanism is outside the scope of this paper.

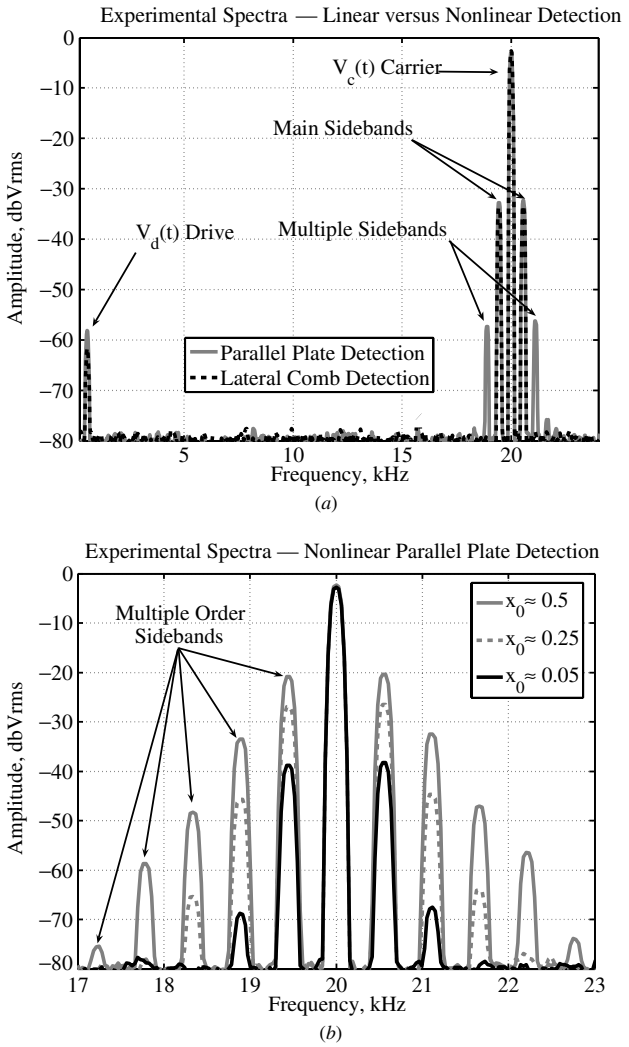

Figure 8. Experimental measurement of linear and parallel plate EAM spectra: (*a*) comparison of linear and parallel plate EAM and (*b*) parallel plate EAM signal at different amplitudes of motion.

4.3. Characterization of parallel plate detection nonlinearities

Figure 8(*a*) shows a comparison of experimentally measured spectra for linear lateral comb and nonlinear parallel plate sense signals for the same mechanical motion. In accordance with equation (18), the parallel plate sense signal contains multiple order sidebands (however, only a limited number of them are large enough to be measured by the equipment). Figure 8(*b*) illustrates this further by comparing spectra of nonlinear sensing at three different amplitudes of motion. Amplitude of any given sideband is an increasing function of the amplitude of motion x_0. For a given amplitude of motion, the amplitudes of multiple sidebands decrease in geometric progression, seen as a linear decay on a logarithmic scale.

A separate set of experiments was performed in order to directly measure the amplitudes of first- (main) and second-order sidebands at different amplitudes of motion. The experiments were similar to the previously described; however, the signal processing was different, see figure 9. The carrier

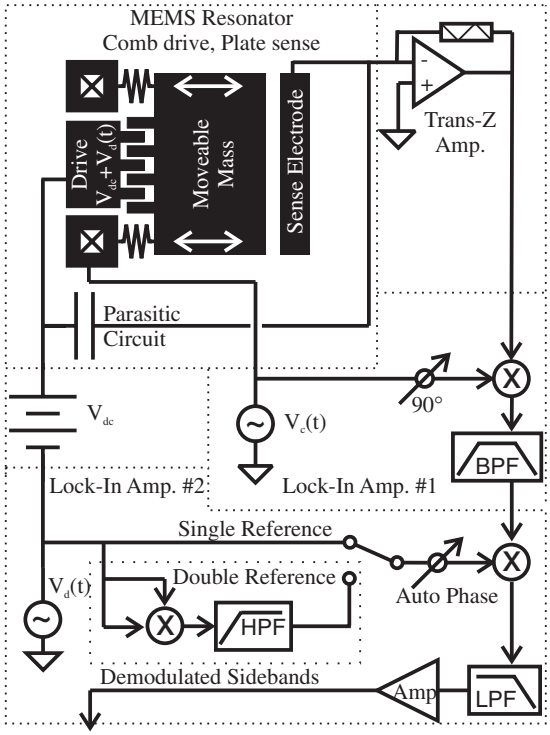

Figure 9. Signal processing diagram for the experimental measurement of nonlinear sidebands.

voltage, generated by the first lock-in amplifier, was applied to the movable mass of the test resonator. The drive voltage was composed of an ac component, generated by the second lock-in amplifier, and a dc component, generated by a separated dc voltage supply. This driving voltage was applied to the fixed lateral comb driving electrode. The anchored parallel plate sense electrode was connected to a trans-impedance amplifier.

The total pick-up current was amplified and converted to a voltage. The first lock-in amplifier demodulated the signal at the carrier frequency with a 90° phase shift of the reference waveform. The obtained voltage was fed into the second lock-in amplifier, which was set up to demodulate at the drive frequency (for the first-order sidebands) or its multiple (for the second-order sidebands). As a result, a dc measurement of the first- and second-order parallel plate EAM sidebands was obtained. This procedure was repeated for different values of the motional amplitude in order to experimentally map $p_{1,2}(x_0)$ and confirm their analytical expressions, see figure 10.

5. Discussions

In this section, we discuss several practical aspects of using the main sidebands of the parallel plate EAM signal for detection of motion in resonant devices.

5.1. Nonlinearity of sensing with pure dc voltage

The nonlinearity of parallel plate sense capacitors also manifests itself in the pick-up signal in the case of pure dc sensing voltage V_{dc}. This approach is often used for sine-sweep characterization of resonant modes (in this case, post-

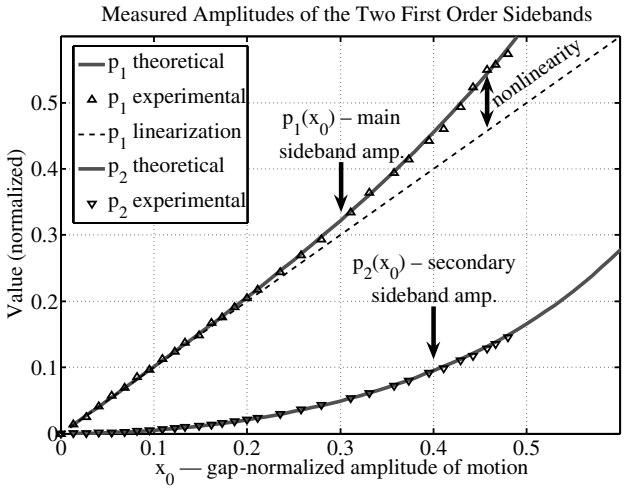

Figure 10. Experimental measurement: nonlinearity of the first two parallel plate EAM sidebands.

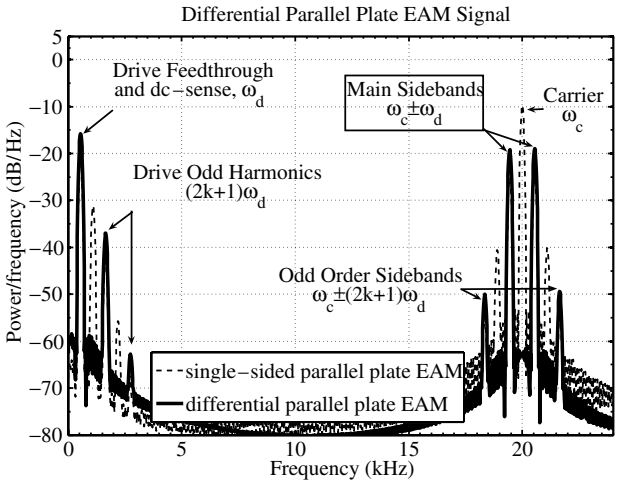

Figure 11. Differential EAM with parallel plates (computer simulation). Spectral profile of differential and corresponding single-sided pick-up signals is shown.

processing is typically required to eliminate the contribution of parasitics [12]). Even though the described configuration does not involve any carrier, it can be conveniently considered a particular case of EAM method with $v_c = 0$. From equation (18), the pick-up signal component caused by the dc sensing voltage is given by

$$I_{V_{\rm dc}}(t) = C_{\rm sn} V_{\rm dc} \omega_d \times \begin{Bmatrix} \sum_{k=0}^{\infty} (2k+1)\, p_{2k+1}(x_0) \cos((2k+1)\omega_d t) \\ -\sum_{k=1}^{\infty} 2k p_{2k}(x_0) \cos(2k\omega_d t) \end{Bmatrix}. \quad (25)$$

Unlike the linear case, the detection of sinusoidal motion with dc-biased parallel plate sense capacitor results in a signal with power at an infinite number of multiple frequencies. The amplitudes of these multiple frequency harmonic signals are proportional to $k p_k(x_0)$. The most power is concentrated at the ω_d frequency; this component is given by $V_{\rm dc} C_{\rm sn} \omega_d p_1(x_0) \cos(\omega_d t)$ equation (25). Similarly to the main pair of EAM sidebands, the amplitude of the ω_d frequency component is a nonlinear function of motional amplitude. The nonlinear dependency is given by the same $p_1(x_0)$. Thus, the presented study of $p_1(x_0)$ and all relevant conclusions are also applicable to the simple detection scheme with a dc bias across the parallel plate sensing capacitor.

5.2. *Differential EAM using parallel plates*

Differential detection schemes are often used in capacitive devices [8, 19, 20]. The total output is formed by the subtraction of two output signals from two identical but oppositely oriented sense capacitors. Ideally, this setup results in the cancellation of common mode parasitic feed-through signals. Next, we analytically investigate the application of a differential EAM sensing configuration to the nonlinear parallel plate detection. We assume a configuration with two identical sense capacitors, $C_{s_1}(t)$ and $C_{s_2}(t)$. They are placed symmetrically, so that both electrodes receive the same amount of the drive and the carrier ac voltages feed-through. These capacitors are also oriented opposite to each other, such that the capacitive gaps change with a 180° phase difference during the motion. The total differential output current $I(t)$ is given by $I_1(t) - I_2(t)$.

The analysis is based on equations (18) and (15). In the case of sinusoidal motion, the two sense capacitances are

$$C_{s1}(t) = \frac{C_{\rm sn}}{1 - x_0 \sin(\omega_d t)}, \quad C_{s2}(t) = \frac{C_{\rm sn}}{1 + x_0 \sin(\omega_d t)}, \quad (26)$$

where the only difference is the sign in the denominators. Since $p_{2k+1}(x_0)$ are odd functions and $p_{2k}(x_0)$ are even functions, the differential output of nonlinear EAM is thus given by

$$I(t) = 2C_{\rm sn} V_{\rm dc} \omega_d \sum_{k=0}^{\infty} (2k+1)\, p_{2k+1}(x_0) \cos((2k+1)\omega_d t) + C_{\rm sn} v_c \sum_{k=1}^{\infty} p_{2k}(x_0) \begin{bmatrix} \omega_{(2k+1)} \sin(\omega_{(2k+1)} t) \\ -\omega_{-(2k+1)} \sin(\omega_{-(2k+1)} t) \end{bmatrix}. \quad (27)$$

Figure 11 illustrates the comparison between parallel plates single-sided and differential EAM sensing schemes. The ideal differential setup cancels out the carrier and the drive feed-through, as well as a half of the multiple frequency harmonics in the spectrum. The odd order drive harmonics and the multiple informational sidebands become doubled in magnitude. Similar to the single-sided sensing case, the first-order informational sidebands are proportional to the nonlinear function $p_1(x_0)$. Thus, both the error analysis, equation (24) and figure 4(*b*), and the proposed methods of the motional amplitude extraction, equation (20) and equation (21), are also applicable to the parallel plate differential EAM scheme.

5.3. *Choice of drive dc-bias application terminal*

Some devices may need a large dc driving voltage component to produce the desired amplitude of motion, see equation (1). This dc bias can be either applied to the resonator's movable mass or to the anchored drive electrode. In the first case, an infinite number of drive harmonics is introduced into the EAM output current due to nonlinearity of the parallel plate capacitors. If the carrier frequency is not chosen properly, one of these drive harmonics can overlap with an informational sideband and corrupt the measurement. This problem can

be avoided by applying the large dc bias to the fixed drive electrode. However, in this case more asymmetry is created in the device, since the movable mass will be pulled toward the anchored drive electrode. To minimize the effect, double-sided actuation, or push–pull architecture, is typically utilized.

6. Conclusions

We presented the complete analytical model for parallel plate capacitive detection of sinusoidal motion with arbitrary amplitudes; the derived model is supported by experimental results. Unlike lateral comb configuration, parallel plate sense capacitors produce a nonlinear detection signal. Fourier series for the parallel plate output signal were analytically derived and studied for the cases of a pure dc sensing voltage, as well as an ac sensing voltage (electromechanical amplitude modulation (EAM)). The nonlinearities of parallel plate EAM were investigated in comparison to the linear case.

Parallel plate capacitor output signal has infinite number of frequencies components, corresponding to multiple order sidebands. Amplitudes of the main informational sidebands (first-order sidebands) are not linear with respect to the amplitude of periodic motion. The degree of sideband nonlinearity increases with the motional amplitude and results in a significant overestimation of the motional amplitude when a linear approximation is used. The nonlinearity of the main pair of the modulated sidebands was investigated in detail. A precise relation between the amplitude of periodic mechanical motion and the amplitude of the sidebands was obtained. Knowledge of this precise relationship allows for elimination of the nonlinearity error in amplitude measurement with parallel plates.

MEMS test structures were designed and fabricated using an in-house SOI process. Experiments confirmed the developed theory of nonlinear detection of motion using parallel plate sense capacitors. Effect of biasing scheme on the output signal was discussed and alternative approaches were compared. Parallel plate sense capacitors are known to provide high capacitive gradient and sensitivity at the cost of nonlinearity error. The proposed algorithms for compensation of the measurement nonlinearity can be used to implement accurate and highly sensitive parallel plate capacitive detection schemes for resonators, gyroscopes and other vibratory MEMS with large amplitude of motion.

Acknowledgments

This work was supported by the National Science Foundation Grant CMS-0409923, BEI Technologies contract BEI-36974 and UC Discovery Program ELE04-10202. We would like to acknowledge Vu Phan of the Integrated Nano-Research Facility (INRF) at University of California, Irvine, for assistance with fabrication, and Max Perez and Adam Schofield of UCI Microsystems Laboratory for stimulating discussions.

References

[1] Lu M S-C and Fedder G K 2002 Closed-loop control of a parallel-plate microactuator beyond the pull-in limit *Solid-State Sensor, Actuator and Microsystems Workshop (Hilton Head Island, SC, USA, 2–4 June 2002)*

[2] Seeger J and Boser B 2002 Parallel-plate driven oscillations and resonant pull-in *Solid-State Sensor, Actuator and Microsystems Workshop (Hilton Head Island, SC, USA, 2–4 June 2002)*

[3] Fargas-Marques A and Shkel A 2005 On electrostatic actuation beyond snapping condition *Proc. IEEE Sensors Conf. (Irvine, CA, USA, 31 October–3 November 2005)*

[4] Trusov A A and Shkel A M 2007 Parallel plate capacitive detection of large amplitude motion in MEMS *IEEE Transducers/Euerosensors 2007 Conf. (Lyon, France, 10–14 June 2007)*

[5] Stemme G 1991 Resonant silicon sensors *J. Micromech. Microeng.* **1** 113–25

[6] Yazdi N, Ayazi F and Najafi K 1998 Micromachined inertial sensors *Proc. IEEE* **86** 1640–59

[7] Turner K K and Zhang W 2001 Design and analysis of a dynamic MEM chemical sensor *Proc. American Control Conf. (Arlington, VA, USA, 25–27 June 2001)*

[8] Baxter L K 1996 *Capacitive Sensors: Design and Applications* (Piscataway, NJ: IEEE Press)

[9] Kovacs G T 1998 *Micromachined Transducers Sourcebook* (New York: McGraw-Hill)

[10] Cao J and Nguyen C-C 1999 Drive amplitude dependence of micromechanical resonator series motional resistance *Dig. of Tech. Papers, 10th Int. Conf. on Solid-State Sensors and Actuators (Sendai, Japan, 7–10 June 1999)*

[11] Acar C and Shkel A M 2005 Structurally decoupled micromachined gyroscope with post-release capacitance enhancement *J. Micromech. Microeng.* **15** 1092–101

[12] Trusov A, Acar C and Shkel A M 2006 Comparative analysis of distributed mass micromachined gyroscopes fabricated in SCS-SOI and EFAB *SPIE Smart Structures and Materials 2006: Sensors and Smart Structures Technologies for Civil, Mechanical, and Aerospace Systems; Proc. SPIE* **6174** 61742A

[13] Tang W C, Nguyen T-C H and Howe R T 1989 Laterally driven polysilicon resonant microstructures *Sensors Actuators* **20** 25–32

[14] Clark W A 1997 Micromachined vibratory rate gyroscopes *PhD Dissertation* University of California, Berkeley

[15] Palaniapan M, Howe R and Yasaitis J 2003 Performance comparison of integrated z-axis frame microgyroscopes *IEEE 16th Ann. Int. Conf. on Micro Electro Mechanical Systems (Kyoto, 19–23 January 2003)*

[16] Nguyen C C 1994 Micromechanical signal processors *PhD Dissertation* University of California, Berkeley

[17] Cagdaser B, Jog A, Last M, Leibowitz B S, Zhou L, Shelton E, Pister K S and Bposer B E 2004 Capacitive sense feedback control for MEMS beam steering mirrors *Solid-State Sensor, Actuator and Microsystems Workshop (Hilton Head, SC, USA, 6–10 June 2004)*

[18] Horowitz P and Hill W 1989 *The Art of Electronics* (Cambridge: Cambridge University Press)

[19] Acar C and Shkel A M 2004 Post-release capacitance enhancement in micromachined devices *Proc. IEEE Sensors (Vienna, Austria, 24–27 October 2004)*

[20] Lemkin M and Boser B E 1999 A three-axis micromachined accelerometer with a CMOS position-senseinterface and digital offset-trim electronics *IEEE J. Solid-State Circuits* **34** 456–68